Certifiable Alignment of GNSS and Local Frames via Lagrangian Duality

Baoshan Song, Matthew Giamou, Penggao Yan, Chunxi Xia, Li-Ta Hsu, *Senior member, IEEE,*

Abstract—**Estimating the absolute orientation of a local system relative to a global navigation satellite system (GNSS) reference often suffers from local minima and high dependency on satellite availability. Existing methods for this alignment task rely on abundant satellites unavailable in GNSS-degraded environments, or use local optimization methods which cannot guarantee the optimality of a solution. This work introduces a globally optimal solver that transforms raw pseudo-range or Doppler measurements into a convexly relaxed problem. The proposed method is certifiable, meaning it can numerically verify the correctness of the result, filling a gap where existing local optimizers fail. We first formulate the original frame alignment problem as a nonconvex quadratically constrained quadratic program (QCQP) problem and relax the QCQP problem to a concave Lagrangian dual problem that provides a lower cost bound for the original problem. Then we perform relaxation tightness and observability analysis to derive criteria for certifiable optimality of the solution. Finally, simulation and real world experiments are conducted to evaluate the proposed method. The experiments show that our method provides certifiably optimal solutions even with only 2 satellites with Doppler measurements and 2D vehicle motion, while the traditional velocity-based VOBA method and the advanced GVINS alignment technique may fail or converge to local optima without notice. To support the development of GNSS-based navigation techniques in robotics, all code and data are open-sourced at https://github.com/Baoshan-Song/Certifiable-Doppler-alignment.**

Index Terms—**GNSS, frame alignment, navigation, sensor integration, convex relaxation.**

I. INTRODUCTION

Localization is an essential capability for any autonomous mobile system [1] including unmanned aerial vehicles (UAVs) [2] and cars used for intelligent driving applications [3]. In localization research, a global navigation satellite system (GNSS) is known to provide globally consistent spatial information in outdoor environments, which is usually employed in multi-sensor fusion approaches to enhance localization consistency and accuracy. Nevertheless, many sensors, such as cameras and inertial measurement units (IMUs), operate by providing measurements in a local frame of reference. In contrast, GNSS works in a global frame fixed to the Earth [4]. To effectively combine GNSS with these sensors, an autonomous localization system must solve an initial frame alignment problem (in both translation and rotation) between the GNSS and local frames. Since GNSS can easily provide globally consistent position [5], the major problem is to estimate the rotation alignment parameters. Therefore, in
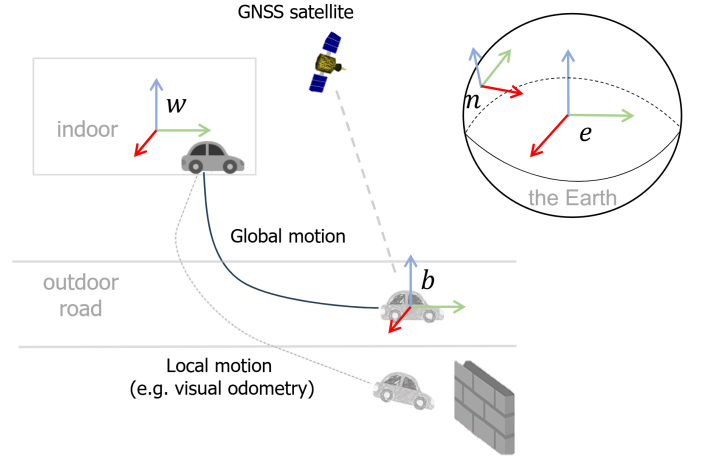
Fig. 1. Illustration of alignment between GNSS e-frame and local w-frame. The key insight is to employ alignment of the local motion and its projection on the GNSS Doppler measurements which implies the global motion.

this work, we refer to the initial rotation alignment between GNSS and local frames as *initial alignment*. Since rotations in three dimensions are described by the nonconvex special orthogonal group (SO(3)), the principal scientific challenge of the initial alignment problem is avoiding local optima which lead to poor alignment performance. To mitigate the effect of nonconvexity, there are plenty of existing works including traditional methods using motion synchronization and advanced methods using raw GNSS measuring models.

A. Traditional alignment methods: closed-form solution

GNSS-aided local frame alignment has been traditionally approached as a motion synchronization problem, i.e., a Wahba problem [6], using motion states such as position [7], velocity [8] and acceleration [9] estimated from a GNSS receiver and other sensors. For instance, optimization-based alignment (OBA) is a term used for systems performing GNSS/IMU integrated alignment [9]. Since there are many mature solutions for motion synchronization, these initial alignment methods can be directly solved by some general registration algorithms, such as singular value decomposition (SVD). For example, the position-based synchronization can be solved by Arun's method to achieve both translation and rotation alignment [10]. Formulations using velocity measurements can also be solved by existing methods, but only provide rotation information [11]. In short, motion synchronization-based methods can be solved to a closed-form optimal solution. However, these methods require abundant (≥ 4) GNSS satellites to provide

motion states as input, which is challenging in GNSS-degraded environments [1]. While simple and optimal, the effectiveness of these methods diminishes under sparse or degraded GNSS conditions, leading to the first research gap.

B. Advanced alignment methods: raw GNSS measurement based methods

To overcome the reliance on rich satellite geometry, recent methods have shifted toward frame alignment using raw GNSS measurements. These include carrier-phase and pseudorange-based positioning, as well as signal shifting measurements such as time-differenced carrier phase (TDCP) [12] and Doppler-based [13] velocity estimation. These methods enable alignment even in low-visibility environments and shorter time spans, by leveraging the geometric consistency between local motion estimates and GNSS observations. However, to the best of our knowledge, there are not closed-form solutions for the alignment problem using raw GNSS measurements, and existing raw GNSS-based methods using local search may converge to local optima when given poor initial guesses. Specifically, these methods offer no optimality guarantees, meaning their convergence is highly sensitive to the quality of the initial guess. Without a certifiable framework, it is impossible to distinguish between a globally optimal alignment and a suboptimal local attractor based on the measurement residuals alone. This leads to the second research gap.

Except from general methods, the extensive body of research on inertial navigation systems (INS) has led to a large number of frame alignment methods designed particularly for inertial sensors. Since a low-cost IMU can provide roll and pitch angles during quasi-static motion by sensing the local direction of the Earth's gravitational field, these alignment methods mainly focus on heading alignment [14], [15]. With determined horizontal angles, the rotation part of the feasible region shrinks from $SO(3)$ to $SO(2)$. This reduction significantly eases the difficulty of local searching, as $SO(2)$ is a minimal degree variety where any non-negative quadratic objective is a sum-of-squares [16]; this geometric property implies a more tractable optimization landscape that allows local search methods to converge to the global optimum with much higher probability.

C. Our porposed approach: convex relaxation with Lagrangian duality

In this work, we aim to bridge these research gaps by developing a certifiable alignment method using raw GNSS measurements that remains robust under partial observability and provides optimality guarantees. To achieve this objective, it is contributive to introduce the growth of convex relaxation.

If a nonconvex problem can be relaxed into a convex problem, it is possible to efficiently find a global optimum. The theory of convex optimization has been studied for decades but limited by computing resources. In recent years, with the rapid evolution of computing devices, advanced optimization methods are leveraged for large scale optimization problems and relaxed problems can be solve efficiently [17]. As a result, in the last decade, convex relaxation has been applied
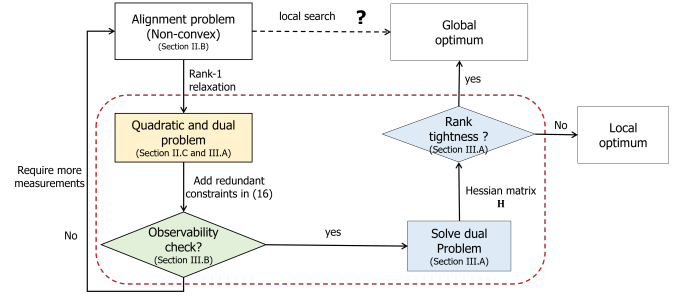

Fig. 2. Pipeline of certifiable alignment

to more robotics problems, such as pose graph optimization (PGO) [18], indoor positioning [19], geometric registration [20], hand-eye calibration [21], rotation synchronization [22], wireless localization [23], camera arrangement [24], orbit determination [25], and opportunistic positioning [26].

This work proposes a certifiable GNSS/local initial frame alignment method using raw Doppler shift measurements via semidefinite programming (SDP). First, we use the GNSS Doppler shift model for alignment and construct a nonconvex QCQP problem. This nonconvex problem is solved using a convex Lagrangian dual relaxation, which we prove is guaranteed to provide a globally optimal solution under explicit observability conditions. To the best of our knowledge, this is the first certifiably optimal GNSS/local frame alignment method using raw GNSS Doppler shift measurements. The contributions are summarized below:

- **Certifiable GNSS-aided alignment method**: a novel estimation method for Doppler-aided GNSS/local frame alignment using convex relaxation. This method provides a solution with an optimality guarantee.
- **Tightness and observability analysis** : relaxation tightness analysis and observability analysis are performed to cope with noisy and degraded measurements in GNSS-degraded environments, such as urban canyons. We find the necessary conditions to guarantee observability and sufficient-and-necessary conditions to guarantee optimality.
- **Experimental evaluation**: both simulation and real world tests are performed to evaluate the proposed method. The results show that our method outperforms the traditional velocity synchronization based method VOBA [8] and the advanced alignment method used in GVINS [14]. We also open-source our code and data for free use by the robotics and autonomous navigation communities.

The remainder of this paper is organized according to the pipeline shown in Fig. 2. Section II introduces the original Doppler-based GNSS/local frame alignment model and construct an equivalent QCQP problem. Section III employs Lagrangian duality to solve the QCQP problem and derive the necessary conditions for optimality and observability. Section V evaluates the performance of the proposed method via simulation and real data. Finally, Section VI discusses our conclusions and future work.

II. PROBLEM FORMULATION

A. Notation

Vectors and matrices are denoted by lowercase and uppercase letters with boldface (e.g. $\mathbf{a}$ and $\mathbf{A}$). A diagonal matrix with diagonal elements $a_1, ..., a_n$ is denoted by $\text{diag}\{a_1, ..., a_n\}$. The i-th to j-th components of $\mathbf{a}$ is denoted by $\mathbf{a}_{(i:j)}$, and the submatrix of $\mathbf{A}$ with corners $(i, i), (i, j), (j, i), (j, j)$ is denoted by $\mathbf{A}_{(i:j)}$. A $n \times n$ identity matrix is denoted by $\mathbf{I}_n$. The rank and trace of square matrix $\mathbf{A}$ are denoted by $\text{rank}(\mathbf{A})$ and $\text{tr}(\mathbf{A})$ respectively. An n-dimension real space is denoted by $\mathbb{R}^n$ and an $n \times n$ symmetric matrix space is denoted by $\mathbb{S}^n$. $\mathbf{A} \succeq 0$ indicates that $\mathbf{A}$ is positive semidefinite and $\mathbf{A} \succ 0$ indicates that $\mathbf{A}$ is positive definite. $\|\mathbf{A}\|$ and $\|\mathbf{a}\|$ denote the 2-norm of a matrix $\mathbf{A}$ and a vector $\mathbf{a}$, respectively. The Frobenius inner product of $\mathbf{A}$ and $\mathbf{B}$ is $\mathbf{A} \bullet \mathbf{B}$. $\otimes$ and $\odot$ denote kronecker and hadamard products, respectively. There are multiple reference frames illustrated in Fig. 1 and their definitions are:

- b: a moving body frame with its origin and directions fixed to the carrier (i.e., right-forward-up (RFU) in this work) [27];
- w: a local world frame fixed to the body frame at the trajectory's start point [14];
- n: a navigation frame with a fixed local origin and geodetic directions (east-north-up (ENU) in this work) [28]; and
- e: a global Earth-centered, Earth-fixed (ECEF) frame with its origin and direction fixed to the Earth [29].

B. Original problem

Our problem is close to the coarse GNSS initial alignment method in GVINS [14]. In GVINS, the yaw offset between the ENU frame and the local world frame is estimated using Doppler measurements. To generalize this method, we extend the Doppler-based rotation alignment between ECEF and local world frame to $SO(3)$ more than yaw offset. According to [30], a typical raw GNSS Doppler measurement model can be written as:

$$\lambda \cdot D = (\mathbf{p}_r^e - \mathbf{p}_s^e)^T (\mathbf{v}_r^e - \mathbf{v}_s^e) / \|\mathbf{p}_r^e - \mathbf{p}_s^e\|_2 + c \cdot \dot{dt}_r + \epsilon, \tag{1}$$

where λ is the wavelength of the GNSS carrier signal (m); D is a Doppler shift measurement (Hz); $\mathbf{p}_r^s$ and $\mathbf{p}_s^e$ are the position of the receiver and the satellite (m); $\mathbf{v}_r^e$ and $\mathbf{v}_s^e$ are the velocity of the receiver and the satellite (m/s); c is the speed of light (m/s); $\dot{dt}_r$ is the clock drift of the receiver; and ϵ is additive Gaussian white noise (m/s). Geometrically, a Doppler shift measurement is the projection of relative velocity on the line of sight vector between a satellite and a receiver [26]. Since a Doppler measurement is generally less noisy than a pseudorange measurement, it can be used to determine the rotation between the ECEF frame and the local world frame $\mathbf{R}_w^e$ using local receiver velocity $\mathbf{v}_r^w$ in the w-frame:

$$\mathbf{v}_r^e = \mathbf{R}_w^e \mathbf{v}_r^w. \tag{2}$$

Also, we simplify the notation of the Doppler shift model with

$$\mathbf{n} \triangleq (\mathbf{p}_r^e - \mathbf{p}_s^e) / \|\mathbf{p}_r^e - \mathbf{p}_s^e\|_2 \tag{3}$$

$$\bar{D} \triangleq \lambda \cdot D - \mathbf{n}^T \mathbf{v}_s^e \tag{4}$$

$$\bar{t} \triangleq c \cdot \dot{dt}_r. \tag{5}$$

Given a bundle of input Doppler shift measurements, satellite positions and velocities from ephemeris, and local velocities at the same time, we can get the Doppler-based GNSS/local frame alignment problem:

$$\min_{\mathbf{R}_w^e \in SO(3), \bar{t} \in \mathbb{R}} \sum_{i=1}^K \|z_i\|_\epsilon^2 \tag{6}$$

where

$$z_i = (\mathbf{R}_w^e \mathbf{v}_{r,i}^w - \mathbf{v}_{s,i}^e)^T \mathbf{n}_i + \bar{t} - \bar{D}_i. \tag{7}$$

Problem (6) is nonconvex since the $SO(3)$ is a nonconvex set. In general, existing local search methods can efficiently find solutions to problems of this form. However, as we will see in our experiments in Section IV, these methods do not have global optimality guarantees and may converge to local minima.

C. Quadratic formulation

To mitigate the shortcomings of local search methods, we can reformulate the cost and constraints of Problem (6) as quadratic forms and employ Lagrangian duality to obtain a convex problem which yields a certifiably globally optimal solution. For the cost function, we can rewrite the original alignment problem with this identity:

$$(\mathbf{R}_w^e \mathbf{v}_r^w)^T \mathbf{n} = (\mathbf{v}_r^w \otimes \mathbf{n})^T \text{vec}(\mathbf{R}_w^e). \tag{8}$$

By reorganizing the variable and coefficient matrix as

$$\mathbf{r} = \text{vec}(\mathbf{R}_e^w) \tag{9}$$

$$\mathbf{m} = \mathbf{v}_r^w \otimes \mathbf{n}, \tag{10}$$

we can write the cost with a homogeneous variable $\bar{\mathbf{r}} = \begin{bmatrix} \mathbf{r}^T & 1 \end{bmatrix}^T$ as

$$\sum_{i=1}^K \|z_i\|_\epsilon^2 = \begin{bmatrix} t \\ \bar{\mathbf{r}} \end{bmatrix}^T \begin{bmatrix} \mathbf{Q}_{t,t} & \mathbf{Q}_{t,\bar{\mathbf{r}}} \\ \mathbf{Q}_{\bar{\mathbf{r}},t} & \mathbf{Q}_{\bar{\mathbf{r}},\bar{\mathbf{r}}} \end{bmatrix} \begin{bmatrix} t \\ \bar{\mathbf{r}} \end{bmatrix}, \tag{11}$$

where

$$\mathbf{Q}_{t,t} = K \quad \text{and} \quad \mathbf{Q}_{\bar{\mathbf{r}},t} = \mathbf{Q}_{t,\bar{\mathbf{r}}}^T$$

$$\mathbf{Q}_{t,\bar{\mathbf{r}}} = \sum_{i=1}^K \begin{bmatrix} \mathbf{m}_i^T & -\bar{D}_i \end{bmatrix}$$

$$\mathbf{Q}_{\bar{\mathbf{r}},\bar{\mathbf{r}}} = \sum_{i=1}^K \begin{bmatrix} \mathbf{m}_i \mathbf{m}_i^T & -\bar{D}_i \mathbf{m}_i \\ -\bar{D}_i \mathbf{m}_i^T & \bar{D}_i^2 \end{bmatrix} \tag{12}$$

To reduce the computational complexity of our method, we can marginalize the clock drift rate t using Schur's complement: the marginalized cost function is

$$\sum_{i=1}^K \|\bar{z}_i\|_\epsilon^2 = \bar{\mathbf{r}}^T \bar{\mathbf{Q}} \bar{\mathbf{r}}, \tag{13}$$

where

$$\bar{\mathbf{Q}} = \mathbf{Q}_{\bar{\mathbf{r}},\bar{\mathbf{r}}} - \mathbf{Q}_{t,\bar{\mathbf{r}}} \mathbf{Q}_{t,t}^{-1} \mathbf{Q}_{\bar{\mathbf{r}},t}. \tag{14}$$

The constraint $\mathbf{R}_w^e \in SO(3)$ is equivalent to [31]

$$SO(3) \equiv \{\mathbf{R} \in \mathbb{R}^{3\times3} : \mathbf{R}^T\mathbf{R} = \mathbf{I}_3, \det(\mathbf{R}) = 1\}. \quad (15)$$

Here the orthonormal constraint is quadratic but the determinant constraint is cubic. According to [31], we can use the quadratic handedness constraints under the right-hand rule to maintain the determinant constraint. We can therefore define the homogeneous variable

$$\mathbf{x} = \begin{bmatrix} \mathbf{r}^T & y, \end{bmatrix}^T$$

and derive a primal QCQP problem equivalent to the original Problem (6):

$$\begin{aligned} \min_{\mathbf{x}} \quad & \mathbf{x}^T\bar{\mathbf{Q}}\mathbf{x} \\ \text{s.t.} \quad & \mathbf{R}^T\mathbf{R} = y^2\mathbf{I}_3, \\ & \mathbf{R}\mathbf{R}^T = y^2\mathbf{I}_3, \\ & \mathbf{R}^{(i)} \times \mathbf{R}^{(j)} = y\mathbf{R}^{(k)}, \\ & y^2 = 1, \\ & \text{with } i, j, k = \mathrm{cyclic}(1, 2, 3). \end{aligned} \quad (16)$$

III. CERTIFIABLE ALIGNMENT

A. Lagrangian duality

To solve the primal QCQP problem, we employ Lagrangian duality to get its dual problem, which is concave with a unique optimum:

$$\max_{\lambda,\gamma,M,N} \gamma \quad (17)$$

$$s.t. \ \bar{\mathbf{Q}} + \mathbf{P}(\lambda, M, N, \gamma) \succeq \mathbf{0}.$$

For details of $\mathbf{P}(\lambda, M, N, \gamma)$, readers can refer to [31]. According to the weak duality theory, the dual problem provides a lower bound of the cost in Problem (6) and its equivalent QCQP (Problem (16). Under some conditions, strong duality exists and we can recover the exact global optimum of the original problem from the dual solution.

The duality gap between the primal and dual cost is an important research topic in the certifiable estimation community. Currently there are two types of commonly used certifiable methods. The first one is to estimate the local optima using local searching methods and certify their optimality using the dual problem. The second one is to solve the dual problem and recover the primal solution. Actually, both of the methods are based on the same sufficient conditions (also sufficient and necessary under low noise disturbance), which is derived from Karush–Kuhn–Tucker (KKT) conditions [32]:

(i) $g_i(\mathbf{x}) = 0, \quad i = 1, ..., 26$

(ii) $\mathbf{H} \succeq 0$

(iii) $\mathbf{H}\mathbf{x} = 0$ where $\mathbf{H} = \bar{\mathbf{Q}} + \mathbf{P}(\lambda, M, N, \gamma)$ is also the hessian matrix of the dual problem (17).

In this work, we take the second type of method since the scale of variables is relatively small and the off-the-shelf convex solver is efficient enough. It is easy to prove our method can achieve zero-duality-gap under noiseless and abundant measurements. Also, the duality is affected by some factors, e.g noises, constraints. We first prove the strong duality with a zero-duality-gap solution under abundant noiseless measurements between problem (16) and (17). Then the measuring

conditions are perturbed to analyze the minimal requirements to maintain the strong duality. The effect of noise has been proved in [32]. The theory has been evaluated in many works, including [18], [21], [33]. Except the disturbance from noises, observability is also an important factor. An frame alignment method is required to be accurate and optimal even with limited measurements. In the following, we focus on the connection between duality gap and observability.

B. Duality gap and observability

Although GNSS provides consistent measurement, its signal could degenerate in blocked environments including urban canyons and forests. Therefore, it is necessary to analyze the duality gap under poor observability conditions. Inspired by some robotic researches, such as [21], [34], it is important to analyze the observability to guarantee the existence of solution. Existing works have shown the benefit of redundant constraints on strong duality [31], [33]. However, this is based on that observability is fulfilled. However, the relationship between redundant constraints and observability is still unclear. Here we focus on the necessary conditions for observability and discuss about the minimum requirements for satellite visibility and motion of the carrier.

Lemma 1 (Necessary conditions of observability with redundant constraints)**.** *The unknown variables in problem (17) with redundant constraints is observable with the Hessian matrix's degree of freedom (DOF) $\geq$ 4. To obtain instantaneous alignment, we need at least 2 satellites and velocity along 2 axis.*

Proof. Given a bundle of Doppler measurements and ephemeris, we can get

$$M_{1:K} = [\mathbf{v}_i \otimes \mathbf{n}_i]_{i=1}^K = \mathbf{V} \odot \mathbf{N} \quad (18)$$

Moreover,

$$\mathrm{rank}(\mathbf{M}) \leq \mathrm{rank}(\mathbf{V}) \cdot \mathrm{rank}(\mathbf{N}) \quad (19)$$

For a Doppler-based alignment problem, there are three unknown variable (three rotation euler angle). Therefore, we require

$$\mathrm{rank}(\mathbf{M}) \geq 3 \quad (20)$$

At the same time,

$$0 \leq \mathrm{rank}(\mathbf{V}) \leq 3, 0 \leq \mathrm{rank}(\mathbf{N}) \leq 3, \quad (21)$$

Hence, the minimum requirement is

$$\mathrm{rank}(\mathbf{V}) \geq 2 \text{ and } \mathrm{rank}(\mathbf{N}) \geq 2 \quad (22)$$

Otherwise, if the rank of any of them is less than 2, the observability requirement is broke. This completes the proof. $\square$

For the observability without redundant constraints, it is more challenging.

Lemma 2 (Necessary conditions of observability without redundant constraints)**.** *The unknown variables in dual problem (17) without redundant constraints is observable with the Hessian matrix's DOF $\geq$ 10, To obtain instantaneous*

TABLE I
SIMULATION TRAJECTORY SETTINGS

Parameter	Value
Interval	1 s
Duration	10 s
Signal Frequency	1575.42 MHz
Receiver velocity	3 m/s
Orbit type	Walker
Clinical angle	55 °
Elevation angle	≥ 10 °

alignment, we need at least 3 satellites and velocity along 3 axis.

Proof. Similar to Lemma 1, for a Doppler-based alignment problem, there are ten unknown variable (nine rotation matrix element and one clock drift rate). Considering the known homogeneous variable, we require

$$\text{rank}(\mathbf{M}) \geq 9 \tag{23}$$

Therefore, the minimum integer rank for $\mathbf{N}, \mathbf{V}$ is full rank:

$$\text{rank}(\mathbf{V}) = \text{rank}(\mathbf{N}) = 3. \tag{24}$$

This completes the proof.   □

IV. EXPERIMENTS

We evaluated the proposed certifiable alignment method through simulation and real-world experiments. Simulations enabled ablation studies on motion patterns, redundant constraints, initial estimates, and noise to assess observability and accuracy. Real-world tests in urban environments demonstrated robustness under realistic GNSS conditions. The method was compared with two Doppler-based baselines. The first baseline is a traditional velocity vector registration approach [8] using SPV velocity estimates [1] aligned via SVD:

$$\min_{\mathbf{R}_w^e \in SO(3)} \sum_{i=1}^{N} ||\mathbf{R}_w^e \mathbf{v}_{r,i}^w - \mathbf{v}_{r,i}^e||_\epsilon^2. \tag{25}$$

The second baseline, adapted from [14], directly uses raw Doppler measurements. Originally for $SO(2)$, we generalized it to $SO(3)$ to handle full 3D rotations. It estimates initial attitude via Gauss-Newton optimization of Doppler residuals across multiple satellites and epochs.

A. Simulation setup

To empirically evaluate the observability lemmas in Section III-B, we designed two simulated trajectories with uniform velocity norms: a 2D planar circular trajectory and a 3D trajectory over a synthetic hill. The detailed configurations for data generation under ideal conditions are summarized in TABLE I. To simulate Doppler shift measurements, GNSS satellites were randomly distributed along a Walker constellation at an altitude of 26,560 km. Satellite velocities were computed assuming uniform angular velocity and governed by the law of gravity, ensuring physically consistent motion.
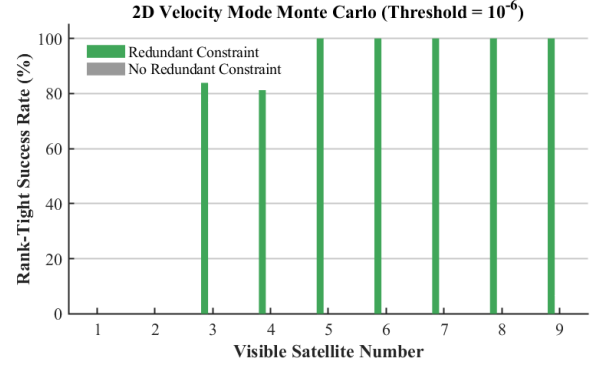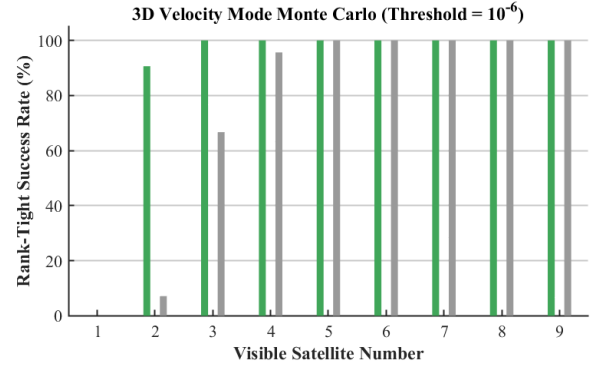

Fig. 3. Optimality success rate in 2D motion. The success is confirmed when the ratio of the smallest eigenvalue to the second-smallest eigenvalue of the Hessian matrix $\mathbf{H}$ is smaller than 10^{-6}.

Fig. 4. Optimality success rate in 3D motion. The success is confirmed when the ratio of the smallest eigenvalue to the second-smallest eigenvalue of the Hessian matrix $\mathbf{H}$ is smaller than 10^{-6}.

Doppler measurements were generated according to the model in (1) with a carrier frequency of 1575.42 MHz.

To mitigate the effects of statistical randomness, each test was conducted 200 times within a Monte Carlo framework to ensure the reliability and reproducibility of the results. Using the resulting simulation data, we performed a systematic analysis across key factors influencing observability and alignment performance, including the number of redundant constraints, satellite visibility, motion modes, initial state guesses, and Doppler measurement noise levels. In Sections IV-B and IV-C, we utilize noiseless measurements to evaluate the optimality of compared methods and the impact initial receiver positions. In Section IV-D, we also assess the robustness of the proposed alignment method and baseline approaches under mild perturbations in the Doppler measurements.

B. Redundant Constraints and Observability

We use noiseless data to illustrate Lemmas 1 and 2, comparing the optimality rate of the proposed method under 3D and 2D motions with varying satellite visibility. Global optimality is confirmed when the SDP solver converges and the Hessian exhibits corank one, numerically verified by the ratio of the smallest to second-smallest eigenvalue below
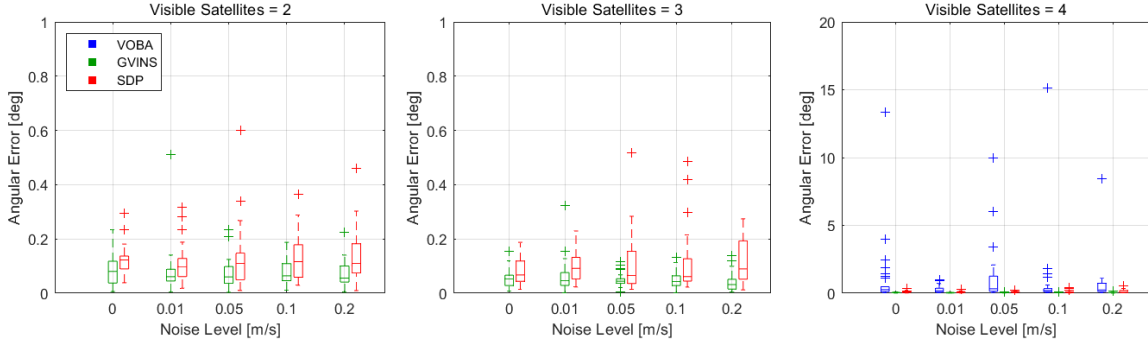
Fig. 5. Doppler noise disturbance test with 3D motion. Noise level denotes the standard deviation of the Gaussian white noise. Alignment error means the rotation error.
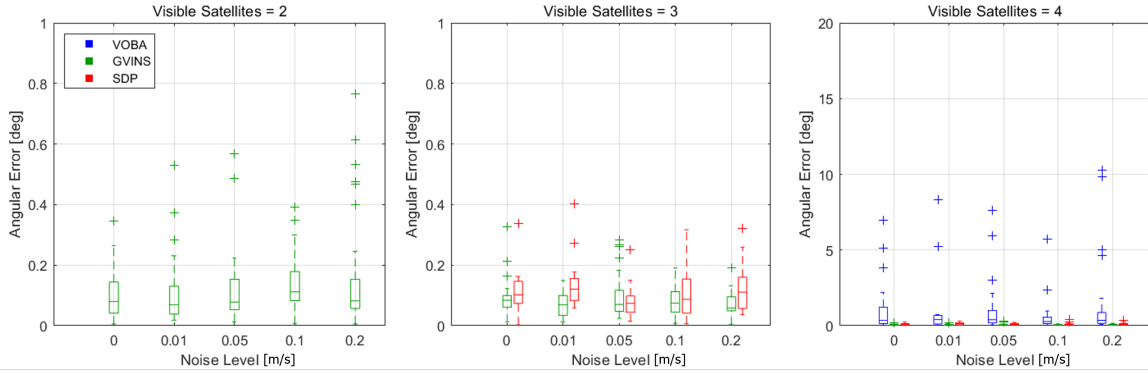

Fig. 6. Doppler noise disturbance test with 2D motion. Noise level denotes the standard deviation of the Gaussian white noise. Alignment error means the rotation error.

10^{-6}. For 3D motion, one satellite yields zero optimality, while two or more satellites with redundant constraints reach 90.62–100%, stabilizing at 100% for five or more satellites. Without redundant constraints, more satellites are needed, and in 2D motion, global optimality cannot be achieved without them, confirming their critical role. These results show that both motion and redundant constraints determine the minimum satellite count for optimality. Consistent with [21], observability and noise affect the zero-gap region, and in some cases, rotation variables are unidentifiable without redundant constraints [33]. Hence, redundant constraints are used by default in our method.

C. Effect of initialization

In this section, we investigate the effect of the initial state estimate on alignment performance. It is worth noting that both the traditional VOBA method and our SDP-based alignment method do not require an initial guess. Therefore, we focus on the advanced alignment method adapted from GVINS, evaluating it under a degenerate condition with an average of only two visible satellites per epoch and randomly initialized states. The results of this evaluation are illustrated in Fig. 7, where the red star represents the ground truth, and the heatmap projected over a unit spherical surface depicts the alignment error across different initializations. Two key observations emerge from these results. First, when the geometric distribution of satellites is poor (e.g. with less than four visible satellites), a high-
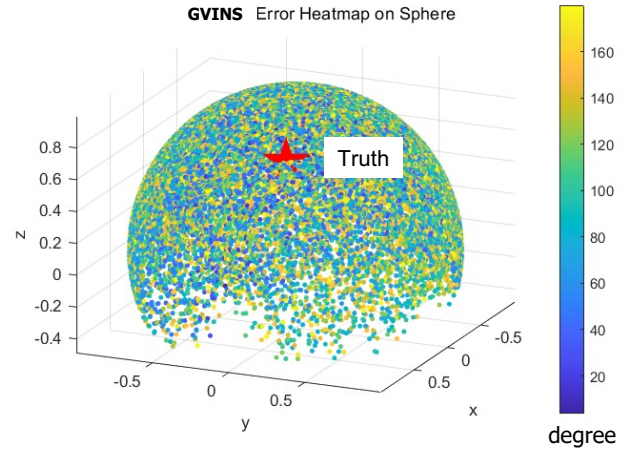

Fig. 7. Under poor observability conditions (defined as two visible satellites), the alignment method in GVINS often converges to local optima from random initializations.

quality initial guess becomes critical for achieving accurate alignment. Second, even initial points located near the ground truth can produce large alignment errors, highlighting the inherent difficulty in identifying feasible initial states under degenerate satellite configurations. These findings underscore the importance of either robust initialization strategies or methods that are less sensitive to the initial guess, particularly
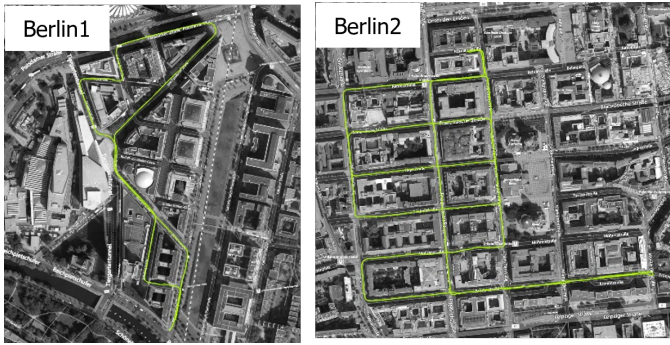
Fig. 8. Dataset scenes and vehicle trajectory (green lines) in the real tests

TABLE II
HARDWARE SETTINGS OF THE REAL TESTS

	Hardware	Features
Ground-truth	NovAtel SPAN	Yaw only
GNSS receiver	U-blox M8T	L1
GNSS Antenna	Patch antenna	GPS, GLONASS measurements (5 Hz)
odometer	CAN	velocity and yaw-rate (50 Hz)

in scenarios with sparse or poorly distributed satellite visibility.

D. Duality gap with noise disturbance

In this section, we evaluate the performance of the GVINS alignment method when provided with the ground truth as the initial state. To investigate the robustness of each method under measurement noise in degraded GNSS environments, we conducted a comparative study among three methods across five different levels of Doppler shift noise. The positioning errors under these disturbances were analyzed separately for 3D and 2D motion trajectories, as shown in Fig. 5 and Fig. 6, respectively. The results indicated that, when exact initial estimates are available, the SDP-based alignment method exhibits mostly the same positioning errors compared to GVINS, both of which had a mean of less than $1°$ across our tests. However, some outliers of the errors of SDP were larger. We speculate that this discrepancy is due to the extreme numerical precision limitations inherent to the interior point solver 'Sedumi' used by CVX [17]. Furthermore, the traditional VOBA method is only able to provide estimates when four or more satellites are visible: with only two or three satellites, VOBA fails to produce a feasible solution. Even when four satellites are available, the VOBA estimates exhibit poor stability and are prone to large outliers, with errors occasionally exceeding $15°$ in attitude estimation. Nevertheless, across all noise levels, the GVINS method maintains stable performance with accurate initialization, demonstrating its effectiveness in coping with Doppler measurement noise, while SDP remains competitive but slightly less precise, which could be improved in future research.

E. Real test

We evaluated the proposed alignment method on the smart-Loc dataset [35], which provides NovAtel SPAN ground truth

and vehicle ego-motion (velocity and yaw rate) from the CAN bus. Low-cost GNSS receivers supply GPS/GLONASS pseudorange and Doppler at L1. Since ground truth only includes heading, we focus on alignment error in this dimension, using a 120-second sliding window for statistics. GVINS is initialized with the identity matrix, and mean processing times per epoch are 0.02 s, 0.02 s, and 0.25 s for VOBA, GVINS, and SDP, respectively.

The results, summarized in TABLE III, include mean absolute errors (MAE), standard deviation of the errors (STD), and maximum errors (MAX). To analyze the effect of sampling frequency, we also downsampled the measurements by a factor of 10 and remarked the tests as Berlin1-10 and Berlin2-10. To demonstrated the influence of satellite visibility, we conducted both *GNSS-healthy* and *GNSS-degradation* tests. In the GNSS-healthy test, we use four satellites per epoch. In the GNSS-degradation test, we restricted the average number of visible satellites to 2 to evaluate the robustness of different alignment methods under limited GNSS conditions. The traditional VOBA method is feasible when sufficient (≥ 4) satellites are employed but fails when fewer than four satellites are visible. Compared to VOBA, the GVINS-based method remains feasible under degraded GNSS conditions but exhibits strong sensitivity to the quality of the initial estimate, especially for degraded cases. Interestingly, downsampling has not influenced the accuracy of VOBA but sometimes affects GVINS. For example, GVINS becomes trapped in local optima in the Berlin2 test but not in the Berlin2-10 test. In comparison, our SDP alignment method remains robust under low satellite visibility and can provide optimality guarantees after estimation.

V. CONCLUSION

In this work, we introduced a certifiable GNSS/local frame alignment method based on Doppler measurements and convex relaxation. By reformulating the alignment task as a nonconvex QCQP and relaxing it into an SDP problem, we established conditions under which certifiable optimality can be guaranteed through relaxation tightness and observability analysis. Both simulations and real-world experiments, including challenging scenarios with as few as two satellites per epoch with 2D motion, demonstrate that our method consistently delivers certifiably optimal solutions where conventional VOBA and GVINS approaches may fail or converge to local optima. To facilitate further research and practical adoption of GNSS-based alignment in robotics, we have open-sourced all of our code and data.

This work shows that, with redundant constraints, an SDP solver is robust to low observability scenarios. Interestingly, these factors are not standalone but affect each other. In future work, we propose to further study the performance of our SDP-based method in degenerated scenarios.

REFERENCES

[1] P. D. Groves, *Principles of GNSS, Inertial, and Multisensor Integrated Navigation Systems*. Boston, MA: Artech House, 2008.

TABLE III
ALIGNMENT ERROR OF THREE COMPARED METHODS IN THE REAL TESTS.

Yaw error [°] MAE/STD/MAX	Ave. Sat. Num.	VOBA			GVINS			SDP		
Berlin1	4	5.76	2.27	11.98	4.72	2.59	10.84	4.69	2.57	9.42
	2	-	-	-	6.05	22.98	172.25	2.64	2.06	7.25
Berlin1-10	4	5.76	2.27	11.98	5.16	3.66	14.57	5.10	3.63	14.33
	2	-	-	-	9.33	25.02	193.91	4.53	3.20	18.55
Berlin2	4	16.19	5.81	23.75	1.46	4.38	106.57	1.29	0.87	3.44
	2	-	-	-	38.90	63.06	168.70	1.60	1.14	4.39
Berlin2-10	4	16.19	5.81	23.75	1.66	1.31	7.79	1.66	1.31	7.79
	2	-	-	-	33.90	61.09	179.17	2.26	1.77	11.98

[2] M. He, C. Chen, J. Liu, C. Li, X. Lyu, G. Huang, and Z. Meng, "Aerialvl: A dataset, baseline and algorithm framework for aerial-based visual localization with reference map," *IEEE Robotics and Automation Letters*, 2024.

[3] T. G. R. Reid, S. E. Houts, R. Cammarata, G. Mills, S. Agarwal, A. Vora, and G. Pandey, "Localization requirements for autonomous vehicles," arXiv preprint arXiv:1906.01061, 2019, available: https://arxiv.org/abs/1906.01061.

[4] C. Chi, X. Zhang, J. Liu, Y. Sun, Z. Zhang, and X. Zhan, "Gici-lib: A gnss/ins/camera integrated navigation library," *IEEE Robotics and Automation Letters*, vol. 8, no. 12, pp. 7970–7977, 2023.

[5] W. Wen and L.-T. Hsu, "Towards robust gnss positioning and real-time kinematic using factor graph optimization," in *2021 IEEE International Conference on Robotics and Automation (ICRA)*. IEEE, 2021, pp. 5884–5890.

[6] G. Wahba, "A least squares estimate of satellite attitude," *SIAM Review*, vol. 7, no. 3, pp. 409–409, 1965.

[7] Q. Chen, H. Lin, J. Kuang, Y. Luo, and X. Niu, "Rapid initial heading alignment for mems land vehicular gnss/ins navigation system," *IEEE Sensors Journal*, vol. 23, no. 7, pp. 7656–7666, 2023.

[8] Q. Zhang, S. Li, Z. Xu, and X. Niu, "Velocity-based optimization-based alignment (vboba) of low-end mems imu/gnss for low dynamic applications," *IEEE Sensors Journal*, vol. 20, no. 10, pp. 5527–5539, 2020.

[9] M. Wu, Y. Wu, X. Hu, and D. Hu, "Optimization-based alignment for inertial navigation systems: Theory and algorithm," *Aerospace Science and Technology*, vol. 15, no. 1, pp. 1–17, 2011.

[10] K. S. Arun, T. S. Huang, and S. D. Blostein, "Least-squares fitting of two 3-d point sets," *IEEE Transactions on Pattern Analysis and Machine Intelligence*, pp. 698–700, 1987.

[11] S. Umeyama, "Least-squares estimation of transformation parameters between two point patterns," *IEEE Transactions on Pattern Analysis and Machine Intelligence*, vol. 13, no. 4, pp. 376–380, 2002.

[12] T. Zhang, S. Liu, Q. Chen, X. Feng, and X. Niu, "Carrier-phase-based initial heading alignment for land vehicular mems gnss/ins navigation system," *IEEE Transactions on Instrumentation and Measurement*, vol. 71, pp. 1–13, 2022.

[13] Y. Wei, H. Li, and M. Lu, "Carrier doppler-based initial alignment for mems imu/gnss integrated system under low satellite visibility," *GPS Solutions*, vol. 25, no. 3, p. 90, 2021.

[14] S. Cao, X. Lu, and S. Shen, "Gvins: Tightly coupled gnss–visual–inertial fusion for smooth and consistent state estimation," *IEEE Transactions on Robotics*, vol. 38, no. 4, pp. 2004–2021, 2022.

[15] T. Li, L. Pei, Y. Xiang, X. Zuo, W. Yu, and T.-K. Truong, "P 3-lins: Tightly coupled ppp-gnss/ins/lidar navigation system with effective initialization," *IEEE Transactions on Instrumentation and Measurement*, vol. 72, pp. 1–13, 2023.

[16] L. Brynte, V. Larsson, J. P. Iglesias, C. Olsson, and F. Kahl, "On the tightness of semidefinite relaxations for rotation estimation," *Journal of Mathematical Imaging and Vision*, vol. 64, no. 1, pp. 57–67, 2022.

[17] S. P. Boyd and L. Vandenberghe, *Convex Optimization*. Cambridge University Press, 2004.

[18] D. M. Rosen, L. Carlone, A. S. Bandeira, and J. J. Leonard, "Se-sync: A certifiably correct algorithm for synchronization over the special euclidean group," *The International Journal of Robotics Research*, vol. 38, no. 2-3, pp. 95–125, 2019.

[19] L. Deng, P. Wei, Z. Zhang, and H. Zhang, "Doppler frequency shift based source localization in presence of sensor location errors," *IEEE Access*, vol. 6, pp. 59 752–59 760, 2018.

[20] H. Yang, J. Shi, and L. Carlone, "Teaser: Fast and certifiable point cloud registration," *IEEE Transactions on Robotics*, vol. 37, no. 2, pp. 314–333, 2020.

[21] M. Giamou, Z. Ma, V. Peretroukhin, and J. Kelly, "Certifiably globally optimal extrinsic calibration from per-sensor egomotion," *IEEE Robotics and Automation Letters*, vol. 4, no. 2, pp. 367–374, 2019.

[22] H. Liu, X. Li, and A. M.-C. So, "Resync: Riemannian subgradient-based robust rotation synchronization," in *Advances in Neural Information Processing Systems*, vol. 36, 2023, pp. 5236–5261.

[23] Y. Yan, G. Yang, H. Wang, and X. Shen, "Robust multiple sensor localization via semidefinite relaxation in wireless sensor networks with anchor position uncertainty," *Measurement*, vol. 196, p. 111193, 2022.

[24] P. Kaveti, M. Giamou, H. Singh, and D. M. Rosen, "Oasis: Optimal arrangements for sensing in slam," in *2024 IEEE International Conference on Robotics and Automation (ICRA)*. IEEE, 2024, pp. 13 818–13 824.

[25] B. Song, W. Wen, and L.-T. Hsu, "Certifiably optimal satellite orbit determination based on doppler measurements for low-earth-orbit satellites," in *2025 IEEE/ION Position, Location and Navigation Symposium (PLANS)*, 2025, pp. 410–416.

[26] B. Song, W. Wen, Q. Zhang, B. Xu, and L.-T. Hsu, "Certifiably optimal doppler positioning using opportunistic leo satellites," *arXiv preprint arXiv:2509.17198*, 2025.

[27] C. Forster, L. Carlone, F. Dellaert, and D. Scaramuzza, "On-manifold preintegration for real-time visual–inertial odometry," *IEEE Transactions on Robotics*, vol. 33, no. 1, pp. 1–21, 2016.

[28] Z. Shen, X. Li, and X. Li, "Advancing high-precision navigation: Leveraging homogeneous sensors in tightly coupled ppp-rtk/imu integration," *IEEE Transactions on Industrial Electronics*, vol. 71, no. 11, pp. 15 100–15 110, 2024.

[29] X. Li, Z. Qin, Z. Shen, X. Li, Y. Zhou, and B. Song, "A high-precision vehicle navigation system based on tightly coupled ppp-rtk/ins/odometer integration," *IEEE Transactions on Intelligent Transportation Systems*, vol. 24, no. 2, pp. 1855–1866, 2022.

[30] F. Guo, Y. Yang, F. Ma, Y. Zhu, H. Liu, and X. Zhang, "Instantaneous velocity determination and positioning using doppler shift from a leo constellation," *Satellite Navigation*, vol. 4, no. 1, p. 9, 2023.

[31] J. Briales and J. Gonzalez-Jimenez, "Convex global 3d registration with lagrangian duality," in *Proceedings of the IEEE Conference on Computer Vision and Pattern Recognition*, 2017, pp. 4960–4969.

[32] D. Cifuentes, S. Agarwal, P. A. Parrilo, and R. R. Thomas, "On the local stability of semidefinite relaxations," *Mathematical Programming*, vol. 193, no. 2, pp. 629–663, 2022.

[33] F. Dümbgen, C. Holmes, B. Agro, and T. Barfoot, "Toward globally optimal state estimation using automatically tightened semidefinite relaxations," *IEEE Transactions on Robotics*, vol. 40, pp. 4338–4358, 2024.

[34] J. Lv, X. Zuo, K. Hu, J. Xu, G. Huang, and Y. Liu, "Observability-aware intrinsic and extrinsic calibration of lidar-imu systems," *IEEE Transactions on Robotics*, vol. 38, no. 6, pp. 3734–3753, 2022.

[35] P. Reisdorf, T. Pfeifer, J. Breßler, S. Bauer, P. Weissig, S. Lange, G. Wanielik, and P. Protzel, "The problem of comparable gnss results–an approach for a uniform dataset with low-cost and reference data," in *Proceedings of the International Conference on Advances in Vehicular Systems, Technologies and Applications (VEHICULAR)*, 2016.